





Anchoring-induced nonmonotonic velocity versus temperature dependence of motile bacteria in a lyotropic nematic liquid crystal

Yu. Faidiuk ^{1,2}, L. Skivka ¹, P. Zelena,¹ O. Tereshchenko,³ O. Buluy ³, V. M. Pergamenschchik,³ and V. Nazarenko ^{3,*}

¹*ESC Institute of Biology and Medicine, Taras Shevchenko National University, Kyiv 03022, Ukraine*

²*D.K. Zabolotny Institute of Microbiology and Virology, NASU, Kyiv 03680, Ukraine*

³*Institute of Physics, NASU, Kyiv 03028, Ukraine*



(Received 8 March 2021; revised 21 September 2021; accepted 27 September 2021; published 5 November 2021)

The elastic and viscous properties of lyotropic chromonic liquid crystals have a very sharp, often exponential temperature dependence. Self-propelled bacteria swimming in this viscoelastic medium induce director deformations which can strongly influence their velocity, and we study the temperature behavior of their motility in the whole range of the nematic phase. We observe experimentally that, with increasing temperature, while the viscosity drops exponentially and the frequency of the flagellum rotation grows linearly, the swimmers' speed first conventionally increases but then, above some crossover temperature, slows down and at the same time bacteria-induced director distortions become visible. It is shown that the physics behind this temperature-driven effect is in a sharp rise in the ability of the bacterium's flagellum to induce director deformations. As temperature increases, the splay and bend elastic constants sharply decrease and the anchoring extrapolation length of the flagellum surface gets shorter and shorter. At the crossover temperature the resulting effective anchoring effect dominates the fast dropping viscosity and the distortion strengthens. As a result, a fraction of the torque the flagellum applies for the propulsion is spent for the elastic degrees of freedom, which results in a bacterium slowdown. To find the director distortions, the flagellum is presented as a collection of anchoring-induced elastic monopoles, and the bacterium velocity is found from the balance of the energy spent for the propulsion and the viscous drag and nematodynamic dissipation.

DOI: [10.1103/PhysRevE.104.054603](https://doi.org/10.1103/PhysRevE.104.054603)

I. INTRODUCTION

Bacteria cannot stay alive in usual thermotropic liquid crystals (LCs). However, living bacteria can be transferred to water soluble nontoxic lyotropic chromonic liquid crystals (LCLCs) and yield highly nontrivial interactions with LC ordering [1–3]. Swarms of bacteria swimming in LCs demonstrate highly versatile and impressive phenomena. Their collective motion can both effectively induce large-scale director patterns such as moving topological defects [4,5] and be in itself directed by the LC director patterns [6,7]. Although microswimmers hardly ever swim alone and their individual swimming patterns are not so spectacular as collective, their individual behaviors are complex [8–10] and understanding the physics related to self-propelled swimmers in both isotropic liquids [11,12] and LCs requires knowledge of their individual behaviors [13–18] (see also numerous references in [18]). The physics of an individual swimmer in a LC medium brings about particular aspects related to the interaction of a swimmer with the LC degrees of freedom and invokes notions traditional to the physics of LCs, such as elastic deformations; different types of viscosities related to the splay, twist, and bend director distortion modes; and surface anchoring. However, LCLCs that can host living bacteria are very special anisotropic media as their elastic and viscous properties

have a very sharp, often exponential temperature dependence [19,20]. At the same time, the investigation of the behavior of anchoring with temperature in a LCLC is lacking. In LCs, the so-called anchoring extrapolation length L_a , defined as the elastic constant-to-anchoring strength ratio K/W , measures the actual ability of a surface to induce LC director distortions: The shorter L_a is, the stronger it is. In a thermotropic nematic LC, L_a is proportional to the scalar order parameter which fully determines its elastic properties. In a LCLC, the situation is much more complex as the length of units, the supramolecular aggregates, that are responsible for the LC nematic order in lyotropic systems strongly depends on the temperature [21]. This difference sharply manifests itself in that the splay and twist elastic constants in a LCLC can vary over a few orders of magnitude, whereas in thermotropic nematic LCs the elastic constants at best can change just a few times. As self-propelled bacteria swimming in this viscoelastic medium induce director deformations which can strongly influence their motility, we have studied the temperature behavior of their motility in the whole range of the nematic phase.

Theoretically, the patterns of individual behavior, propelling efficiency, orientation with respect to the director, the speed of translational, rotational, undulatory, and whatever other possible ways for an individual bacterium to move in a LCLC and the velocity field of LC fluid induced thereby are all interconnected. They depend on a large number of parameters which can hardly be consistently incorporated in the framework of a single approach [13–18]. Nor can such

*vnazaren@iop.kiev.ua

complex interplay of different parameters be addressed in the course of a single experiment. In this paper we study the temperature-driven effect on a bacterium *Proteus vulgaris* which self-propels by rotating a flagellum attached at its end and deal with the most obvious and physically important parameters of its behavior in a disodium cromoglycate (DSCG) LCLC. These are the bacterium velocity and frequency of the flagellum rotation, the elastic constants and viscosities of the LC host, the anchoring at the flagellum's surface, the bacterium's size and other geometrical characteristics, and distortions of the nematic director behind the rotating flagellum [9], which are not always observable but are always induced and contributing to the motility. This approach proves to be fruitful: We find an unexpected temperature effect on the bacterium motility which is brought about by the interplay of the viscosity, elasticity, and anchoring in a LCLC and sheds light on their causality.

The conventional knowledge is that usually bacteria swim faster at higher temperature T . Biologists had found long ago that in isotropic liquids bacteria show a higher motility at higher T , e.g., as T increases from 10 °C to 50 °C, the speed of many kinds of bacteria increases about five times [22]. Of course, due to purely physiological, intrinsic reasons bacteria can swim slower at higher temperature. For instance, when nutrients are scarce in the environment the bacteria's intracellular pH can decrease with temperature; then their flagellum rotation frequency drops and as a result their velocity decreases [23]. However, this specific biological effect is not connected to the external physical conditions and, as shown below, is not related to the bacteria's slowdown reported here.

At the same time, the T dependence of bacterium motility in a LCLC has not been investigated closely. The most comprehensive studies of temperature effects in LCLCs were presented in Refs. [19,20], where the T dependences of the splay, twist, and bend elasticity and viscosity were measured in detail in the temperature interval from 19 °C to 30 °C. Other reported relations of interest here are as follows. The velocity of *Proteus vulgaris* in a DSCG LCLC at room temperature is proportional to the frequency f of the flagellum rotation [8]. Elongated bacteria usually (but not always; see, e.g., [24]) align with and swim along the local nematic director orientation [8–10]. Distortions of the nematic director behind the bacteria can be visible and used to measure the frequency of the flagellum rotation [9]. Biologists have also established that the effective surface density of flagella is important: The motility is only slightly affected by the cell length, but is considerably strengthened by the density increase of its flagella [25]. In theoretical motility models of flagellated bacteria the surface density of flagella is translated into their thickness; hence thicker flagella result in a higher bacteria speed as they have a higher surface area. Finally, it has been established that the velocity is a decreasing function of the effective viscosity η_{eff} experienced by a moving bacterium [26], which is intuitively understandable because the drag force must be higher in a more viscous medium. However, our findings show that the viscosity-velocity relation in a LCLC can be more complex.

For our studies we used rod-shaped multiflagellated bacteria *Proteus vulgaris* Hauser 1885 B-905^T, which is justified by the unique behavioral patterns. First, stochastic run-

and-tumble multidirectional movement (chemotactic motion) called swimming is characteristic of these multiflagellated bacteria in isotropic environments [27,28]. Second, switching to swarming ability, i.e., a collective motility associated with the change of short swimmer cells into long, polyploid, and hyperflagellated swarmer cells, is inherent to the genus *Proteus* [29]. It gives us the possibility to explore the effect of morphological heterogeneity of bacterial cell population on its motion within anisotropic environments. We investigate the temperature dependence of the effective viscosity η_{eff} , velocity v , and flagellum frequency f of different size bacteria in the interval from 5 °C to 35 °C. It is found that the speed $v(T)$ initially almost linearly increases but then attains a maximum at some crossover temperature $T_c \sim 15$ °C and slowly decreases afterward. At the same time, the frequency $f(T)$ is linearly increasing and the viscosity $\eta_{\text{eff}}(T)$ is exponentially dropping in the entire temperature interval. Thus, only initially is the dependence v vs η_{eff} conventionally increasing, but for $T > T_c$ the regime is decreasing. Such an unusual (unconventional) type of the velocity versus viscosity relation was, as mentioned above, observed in [23] and also recently was predicted for an artificial swimmer with an intrinsic elastic degree of freedom in [30] and called aberrant. We stress that our bacteria do not have such intrinsic degrees of freedom and the situation and problem described in Ref. [23] substantially differ from those in our study. In [23] the speed for a low nutrient starts to decrease as T increases because the rotation frequency f is decreasing, and the task is to explain why f is decreasing. In our study, f is increasing for all T and the task is to explain why f is increasing but nevertheless the speed is decreasing. Thus, the mechanisms behind the bacteria behavior in [23,30] are not related to our problem and cannot be alternative explanations of the effect presented in our paper.

In Sec. II we describe sample preparation, bacteria observation, and the experimental T dependences obtained. Section III presents our theoretical consideration of the flagellum-induced director deformations and the derivation of the $v(T)$ dependence that is in line with the experiment. We show that, at the crossover temperature, the increase of the effective anchoring effect due to the sharp drop of the splay elastic constant dominates the fast dropping viscosity effect. As a result, the director distortion strengthens and a fraction of the torque the flagellum applies for propulsion is spent for the elastic degrees of freedom, which results in a bacterium slowdown. This section includes a brief account of the known theoretical results to show the context within which our theory is developed. Section IV contains a brief conclusion.

II. EXPERIMENT

A. Materials and sample preparation

1. Bacteria and their cultivation

We used the *Proteus vulgaris* Hauser 1885 UKM 412-905⁴²² strain, provided by the Institute of Microbiology and Virology of the National Academy of Sciences of Ukraine. It is a highly motile peritrichous gram-negative non-spore-forming facultative-anaerobic pleomorphic indole-producing bacterium. For bacterial cultivation and as a LC solvent the following liquid media were used: terrific broth (TB)

(Sigma-Aldrich) without glycerol addition, terrific broth supplemented with 0.8% glycerol, nutrient broth (Himedia), nutrient broth supplemented with 2% peptone, lysogeny broth (LB) (Sigma-Aldrich), lysogeny broth with 0.1% glucose, meat peptone broth, casein mannitol metal medium (CMM), and motility buffer (MB) (10 mM KPO_4 , 0.1 mM ethylenediaminetetraacetic acid, 10 mM lactic acid, and 20 mM glucose). For the bacteria propagation on solid media, either nutrient agar (NA) (Himedia) or a relevant liquid medium with agar (0.3–1.5%) were used. Media were sterilized by autoclaving (as defined by the manufacturer), with heat-labile components being added afterward. Exceptions were CMM and MB that were sterilized by filtration.

The procedure of bacterial culture preparation for the growth curve obtention was as follows. The center of a partially dried NA plate was inoculated with a loopful of bacterial cells. After incubation for 24 h at 34 °C, a loopful of cells was taken from the plate edge (to collect highly mobile forms) and introduced into 2 ml of relevant liquid growth medium in a 10-ml flask. The flasks were then cultured under forced aeration at 34 °C for 16 h using an ES-20 (BioSan) orbital shaker incubator (220 rpm). Next the 16-h culture was introduced into a relevant fresh growth medium at a dilution of 1:100. Then 200 μl of the resulting cell suspension was added to the wells of a 96-well plate in three replicates. The growth kinetics of the culture at 34 °C was determined using Bio-Rad Microplate Reader (USA) at a wavelength of 578 nm for 20 h. According to the obtained readings of optical density dependence on cultivation time, the growth curve for each tested growth media was plotted. All experiments were conducted at least in triplicate.

The precultivation of the bacterial culture was similar to those described above. It involved 1:100 dilution of the 16-h culture in 2 ml of relevant fresh media in a 10-ml flask followed by the incubation with aeration at 34 °C for 3 h. Bacterial cells were centrifuged for 10 min at 3000 rpm and gently resuspended in a liquid medium or buffer up to an optical density of 0.8. Finally, 10 μl of obtained cell suspension was introduced into a dissolved LC or liquid medium for motility studies.

2. LC and sample preparation

The LCLC was prepared from an aqueous solution of the cromolyn disodium salt hydrate (DSCG) obtained from Spectrum (TCI Europe N.V., CAS RNff1a15826-37-6, product No. C2521). DSCG is a well-known LC material and has already been characterized in a number of works (see, e.g., [21,31]). At room temperature, the aqueous solution of DSCG is in the isotropic phase for the weight concentration of the materials up to 10 wt.%. In the range of 10–12 wt.%, the solution demonstrated a wide biphasic region of coexisting nematic and isotropic phases. The nematic *N* phase was observed for a range of concentrations of about 13–17 wt.%. For higher concentrations, another biphasic region with coexisting nematic *N* and *M* phases was observed. DSCG is nontoxic and can be in contact for a long time with biological organisms such as floating bacteria. DSCG of 98% purity was dissolved in a selected culture medium at a concentration of 17 wt.%. To obtain the desired working concentration (in our case it is

16 wt.%) of DSCG, a concentrated suspension of bacteria and, if necessary, a liquid culture medium was added to the original suspension of DSCG.

The uniform surface alignment of the *N* phase was achieved by buffed polyimide layers. We used spin-coated and buffed films of chemically imidized polyimide LARC CP1 [32]. The glass with transparent indium tin oxide coating was washed in an ultrasonic cleaner for 15 min, rinsed in deionized water, rinsed with isopropyl alcohol, blown off with nitrogen, and baked at 150 °C for 20 min. The alignment films were deposited by spin coating 0.5% solution of LARC CP1 in the methyl ethyl ketone. The coated glass was baked at 105 °C for 30 min to bake off the solvent. The polyimide-coated glass plates were rubbed and assembled with antiparallel rubbing directions. The thickness of the LC layer was set at 10 μm by calibrated glass spheres. The pretilt angle measured between the director and the substrate was less than 1°.

B. Bacteria observations

For tracking of bacteria trajectories, we used a camera equipped with a monochrome CCD attached to an Olympus BX53 polarizing optical microscope. The camera was connected to a computer via high-speed FireWire 400 data link (IEEE 1394 interface). The camera provided a maximum frame rate of 2500 frames/s and a time resolution of 0.4 ms. A single video image has typically 128×128 pixels with 256 gradations of gray (8 bits per pixel). The pixel size is 6.7×6.7 μm^2 . The microscope is equipped with a 40× long-working-distance objective (numerical aperture equal to 0.5) with manual adjustments for different cover slip thicknesses. The magnification was 168 nm/pixel and the Airy disk of diffraction was about ten pixels across. The temperature was controlled with an Instec HS-1 heating stage providing temperature stability and accuracy of 0.1 °C.

Transmission electron microscopy (TEM) for cell visualization was performed as described previously [33]. For the TEM study, bacteria were cultured as described above for the LCLC experiment and sampled from the broth at the time point of the cell harvesting (without sedimentation). Bacterial cells were absorbed onto the Formvar-coated copper grids for 20 min (grids floating on a top of suspension drop) and then, in a similar way, washed thrice with deionized water for 30 s. Negative staining was performed applying 2% uranyl acetate, for 45–55 s, followed by a second washing step (deionized water, thrice, for 30 s). Air-dried grids were examined using a JEOL JEM TEM1400 transmission electron microscope at magnification of up to 12 000×. Cell parameters were measured with IMAGEJ and FIJI.

C. Experimental results

The first task of our study was to choose the optimal growth medium for bacteria cultivation in order to obtain highly active and motile organisms for the LC experiment, considering the great diversity of media or solvents used by different research groups [8–10,26]. For this purpose, we examined the growth kinetics and morphology (size range and flagellation) of *Proteus vulgaris* Hauser 1885 UKM 412-905^T cultured in seven liquid nutrient media most commonly used in the

TABLE I. Ability of bacterial cells to move in isotropic or anisotropic conditions: + denotes high motility (more than 90% of bacteria are motile) and – low motility (bacteria do not move or the motility of bacteria is low).

Medium of cultivation	Medium for LCLC preparation			
	Nutrient broth	Terrific broth with 0.8% glycerol	Lysogeny broth	Terrific broth without glycerol
Nutrient broth	+/-	+/-	+/-	+/-
Terrific broth with 0.8% glycerol	+/-	+/-	+/-	+/-
Lysogeny bath	+/-	+/-	+/-	+/-
Terrific broth without glycerol	+/-	+/-	+/+	+/-

experiments concerning bacteria motion in LCs. The motility of the bacteria in isotropic and anisotropic surroundings is summarized in Table I. The microorganisms were motile in all investigated isotropic media. However, in anisotropic LCLCs the cells motility was significantly reduced. The bacteria remain motile only in the system of precultivation in TB without glycerol and inoculation of crystal solution in LB. Note that motile cells were actually observed in each case, but the ratio between motile and nonmotile bacteria was rather low for reliable experiments. Positive motility in Table I indicates that more than 90% of cells demonstrate active movement. Thus, in further studies, we used a TB medium without glycerol to preculture the cells and a LB medium to prepare the crystal solution with active bacteria. We shifted the time point of cell harvesting from the commonly used late exponential phase [8,19,26] to the mid logarithmic phase considering highest bacteria motility during this time period [34].

The motility of *Proteus* genus is stipulated by its peritrichous flagellation. Due to its pleomorphic nature these bacteria may exist both in the form of motile sparsely flagellated swimmer rod-shaped cells of 1–10 μm size and in the form of long filamentous hyperflagellated cells known as swarmer. As one can see in Fig. 1, cells of *Proteus vulgaris* Hauser 1885 UKM 412-905^T sampled in the mid logarithmic phase varied significantly in length and the number of flagella. In this heterogenic cell population, four groups were qualitatively defined according to the cell length and flagellation features, which probably represent different stages of transition from swimmer to swarmer (Fig. 1). This transition includes cell elongation, progressive flagellation increase, and motility enhancement [29]. The largest group (~87%) was represented by weakly flagellated (five flagella per cell) cells with an average length of 3 μm (Fig. 2). The second group (~12.0%) included bacterial cells with an average length of 6 μm and slightly increased flagellum number. The third group (~4%) included moderately flagellated cells of average length 9 μm . The fourth group, the smallest one (~0.3%), was represented by elongated (average length 12 μm) hyperflagellated cells.

Microscopic observation of bacteria in a LCLC reveals a variety of cell lengths in the same range from 3 to 12 μm , but here the size distribution is very different (Fig. 2). The distribution was calculated for cells captured within the area of one microscopic view for four different samples taken at the same concentration of DSCG and temperature. As compared to an isotropic liquid host, bacteria in LCLCs are characterized

by a noticeably increased number of large hyperflagellated cells.

Previous reports have shown that the motility of bacteria in anisotropic liquid (water solution of DSCG with concentration above the isotropic-nematic transition) is in general within a window of 2–25 $\mu\text{m}/\text{s}$ [8,9,26]. If we consider bacteria of different size groups separately and measure their mean speed we can get a more uniform velocity distribution. Figure 3(a) presents the temperature dependence of the mean speed for cells of different size groups. To avoid a large error in the speed distribution, we eliminated 10% of the fastest cells and 10% of the slowest from all tracked bacterium trajectories.

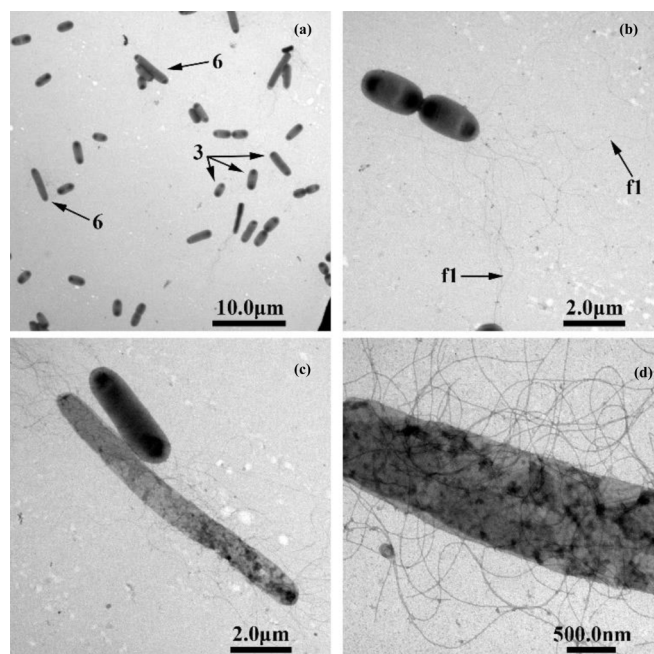


FIG. 1. TEM image of bacteria at the time of cell harvesting for LC inoculation (middle logarithmic phase, 3 h of cultivation in TB liquid medium). (a) General view. Cells sizes are 3 and 6 μm (marked with arrows 3 and 6, respectively) and the scale bar is 10 μm . (b) Cells of 3 μm size, arranged in pairs. The flagellum length (arrow marked with fl) significantly exceeds the cell's length; the scale bar is 2 μm . (c) Moderately flagellated 9- μm cell next to a 3- μm cell; the scale bar is 2 μm . (d) Fragment of a large 12- μm hyperflagellated cell. Multiple flagella of this size bacteria are visible; the scale bar is 0.5 μm .

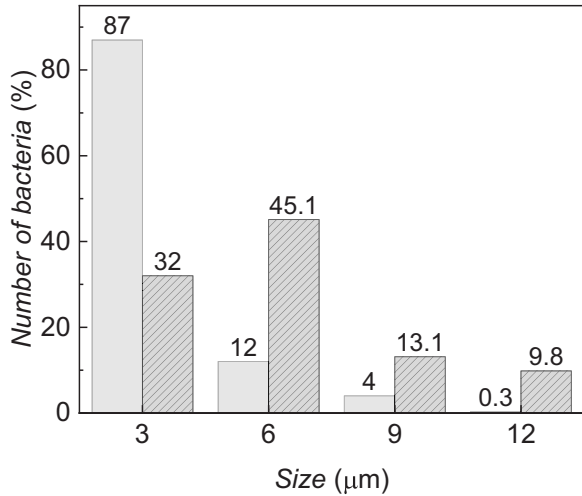


FIG. 2. Distribution of bacterium lengths in a TB liquid medium (light gray shaded columns) and in the 16 wt. % water solution of DSCG (hatched columns).

Finally, to obtain an average over the ensemble distribution we analyzed around 140 trajectories for small size cells (3- and 6- μm groups) and more than 160 trajectories for large size cells (9- and 12- μm groups). In [8], cells of smaller size were reported to be faster than larger ones as they possess a more optimal force-to-drag ratio. In contrast, we observed that the larger cells move faster than the smaller ones, which correlates with the data of another research group [35]. This is presumably because in our experiment a high density of flagella (typically characteristic of elongated cells) rather than cell shape was the primary actor stipulating higher bacterium velocity in fluids of increasing viscosity [25].

The planar anchoring at the surfaces of the elongated bacteria's bodies aligns them along the director. As a result, flagella's axes and bacteria's speeds are also aligned along the nematic director. The main challenge of our experiment was to obtain the dependences of an effective viscosity along the director and of the speed and flagellum rotation frequency on temperature T and at the same time to try to detect their possible correlation with visible elastic distortions. It has been known that some swimming bacteria leave visible traces of director distortions [7,10]. The visibility of traces depends on many factors and not all bacteria of similar size and speed leave them. Nevertheless, we observed a clear correlation between the probability of appearance of such traces for 12- μm and 9- μm bacteria and the point where the speed versus temperature dependence undergoes a substantial change. We performed our experiments using the temperature as a control parameter which varied in the range 5°C–35°C in a 16 wt. % DSCG-water solution.

Measurement of an effective viscosity $\eta_{\text{eff}}(T)$ for a given cell at fixed T in an ideal experiment would require finding its speed along the director for known drag force, which we find impossible. At the same time, the information which is most important to our task is contained in the temperature dependence that is expected to be practically universal for bodies the size of bacteria, and we measured $\eta_{\text{eff}}(T)$ for a ball. To obtain this effective viscosity $\eta_{\text{eff}}(T)$, at fixed T , we recorded the

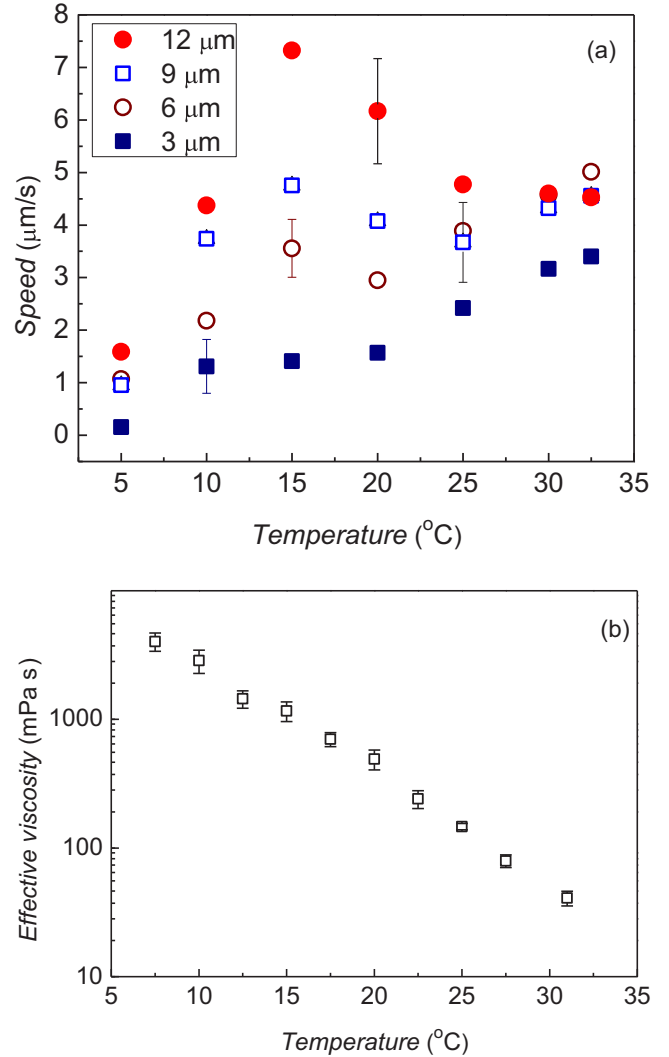


FIG. 3. (a) Temperature dependence of the mean speed for bacteria of different sizes. Velocities for 3 and 6 μm sizes are taken for 140 bacterium trajectories. For larger 9- and 12- μm cells, the averaging was performed over an ensemble of 160 trajectories. (b) Effective viscosity of DSCG-water solutions as a function of temperature.

time required for a 5- μm silver ball to fall along the director under gravity force F_g through the oriented DSCG layer and averaged it over the results of three tests. The viscosity was then found from the formula $F_g = 6\pi\eta_{\text{eff}}R_bv$, where R_b and v are the ball radius and experimentally measured velocity along the director, respectively. The detected dependences of cells' speed and effective viscosity on temperature are presented in Figs. 3(a) and 3(b), respectively. For our 16 wt. % nematic DSCG, at $T = 25^\circ\text{C}$, $\eta_{\text{eff}} \simeq 1.1$ Pa s, which reasonably agrees with the value of approximately 1 Pa s found in [10] from rheological measurement for a 15 wt. % nematic DSCG. The effective viscosity exponentially drops in the total range of T similarly to the splay and twist viscosities [19]. In contrast, the velocity demonstrates a more complex behavior that has not been observed in similar systems.

The velocity of 3- μm cells monotonically increases with temperature, but the increase of speeds of the 6-, 9-, and 12- μm cells ends at the maxima which all are located

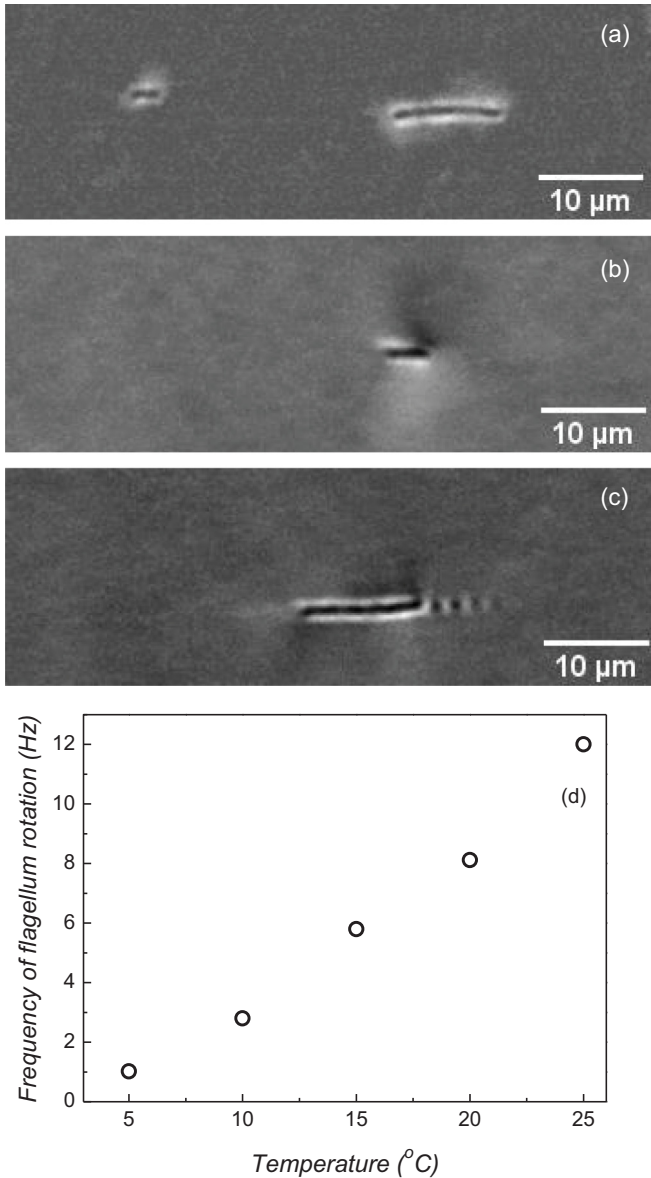


FIG. 4. Microscopic picture of moving bacteria. (a) Bacteria of small 3 μm and large 12 μm size at $T = 5^\circ\text{C}$. There are no visible director distortions along the bacteria's traces. Bacteria of (b) 3 μm and (c) 12 μm size at higher temperature $T = 20^\circ\text{C}$. Director distortions are clearly visible behind the 12- μm cells at $T > 15^\circ\text{C}$. (d) Frequency f of flagellum rotation as a function of temperature.

approximately at $T_c \sim 15^\circ\text{C}$. Thus, the speed is a monotonically increasing function of viscosity only for 3- μm cells, whereas for the larger cells, as T passes the crossover point T_c this conventional regime changes to an aberrant regime in which speed is lower for lower viscosity. Moreover, while the 3- μm cells do not leave a visible trace in the whole T interval, the larger cells start to generate progressively more visible traces as their speeds pass the maxima at T_c [Figs. 4(a)–4(c)]. Of course, all cells generate director distortions of some magnitude, but not all cells, even of large sizes, generate visible traces. We observed that larger cells leave more visible traces. As T approaches T_c the percentage of cells with visible traces substantially increases. At $T = 17^\circ\text{C}$ these were 12%, 50%,

and 97% for 6-, 9-, and 12- μm cells, respectively. The results presented in Fig. 4(d) were obtained by averaging over the numbers of trajectories which were different for different T . As for low $T = 5^\circ\text{C}$, 10°C , and 15°C , a fraction of bacteria that leave visible director distortions is small and as small 3- and 6- μm bacteria do not leave visible traces, for these T the averaging was performed over ten measurements with 9- and 12- μm bacteria. For higher $T = 20^\circ\text{C}$ and 25°C , we analyzed trajectories of 6-, 9-, and 12- μm bacteria and their number increased to 20.

We see that, in the aberrant regime, practically all of the largest 12- μm cells generate visible traces behind their bodies. As a small fraction of these cells also have less visible traces at lower temperatures, we were able to measure the frequency of modulation of the trace brightness for all temperatures. This frequency of the flagellum rotation f was measured by monitoring that of bright spot alternation at a fixed distance from the cell and is presented in Fig. 4(c). Thus, our observations show a clear correlation between the crossover point and the onset of the generation of visible traces. This is a strong indication that the speed slowdown of larger cells as the viscosity continuously drops is related to the loss of propulsion energy due to the elastic degrees of freedom of the LC medium. The experimental data presented in Fig. 3(a) for 12- and 9- μm cells are used in the next section, where the theory of the observed effect is presented.

III. ELASTIC CONTRIBUTION TO THE FLAGELLUM TORQUE AND NONMONOTONIC SPEED VERSUS TEMPERATURE DEPENDENCE

A. General idea and energy balance

Our task here is to explain the observed behavior of the bacterium speed as viscosity drops with the temperature increase. The speed versus viscosity behavior is nonmonotonic and consists of a conventional increasing regime and an aberrant decreasing regime, separated by a crossover point at about $T \sim 15^\circ\text{C}$. As the velocity decrease appears along with the elastic deformation visualized by the traces behind moving cells and as such traces are left by (predominantly) large bacteria, the physics behind the observed effect is expected to be connected with the cells' size and their ability to distort the LC director. Hence, the energy of the rotating flagellum is dissipated by the standard viscous drag as well as by the nematodynamic drag which is due to the induced director distortions, and the balance determines the propulsion speed. The latter dissipation source requires finding the director distortions induced by the anchoring on the surface of the rotating flagellum and their contribution to the dissipation. This problem has not been addressed in the literature.

Simultaneous incorporation of the anisotropic viscosity, realistic bacterium motion pattern, and the elastic, hydrodynamic, and nematodynamic response to this motion is a formidable theoretical problem. For this reason, to better understand how anisotropy affects propulsion in a nematic LC, the above problem has been addressed for the model of a sheet supporting small-amplitude traveling waves, also known as the Taylor swimmer [13,16,17], or for the so-called minimal active model [18,36]. As the observed cells' behavior suggests

that swimming in an anisotropic medium can conveniently be utilized to direct the motion of self-propelling active agents, these studies mostly focused on the orientation of different swimmers with different surface anchoring with respect to the nematic director. Moreover, in a certain respect, it is this orientation that has often been associated with the individual behavior of swimmers in a nematic LC [8,14,24]. Our interest in the interplay between viscosity, elasticity, and director distortions is motivated by the experiment in which the problem is not the bacterium orientation with respect to the LC director (it is just known) and by the specific physical effect presented in this paper, and our theoretical problem is substantially different.

A bacterium exerts a torque Γ on its flagellum and rotates it with frequency f . The flagellum will be assumed to have a circular cross section of radius R_0 and form a perfect spiral of radius R , period $L = 4R \cot \psi$, and the number of periods m , where ψ is the constant angle made by the local flagellum axis \mathbf{l} and the unperturbed director \mathbf{n}_0 (Fig. 5). The friction between the beating flagellum and liquid results in a thrust force and the bacterium moves with a certain translational velocity \mathbf{v} [11,12]. In line with the experimental situation, the bacterium body and its velocity \mathbf{v} are parallel to the uniform director \mathbf{n}_0 imposed by the sample's boundaries. In addition to the translational velocity \mathbf{v} , there is certain small stationary rotational velocity component \mathbf{v}_{rot} about the spiral's axis. If, as usual [11,12], we disregard end effects related to the finite flagellum length, then \mathbf{v}_{rot} depends only on the distance from this axis. The total velocity $\mathbf{u} = \mathbf{v} + \mathbf{v}_{\text{rot}}$ is the sum of contributions induced by every small flagellum element due to the viscous friction [37,38]. In addition, due to surface anchoring, the surface of every small flagellum element induces a weak director distortion; the homogeneous director \mathbf{n}_0 changes by $\delta\mathbf{n}$, so the total director $\mathbf{n} = \mathbf{n}_0 + \delta\mathbf{n}$. Consequently, there are two sources of energy dissipation as the bacterium moves through a LC.

Under the above assumptions, the energy conservation, which requires that the bacterium energy output $dE/dt = 2\pi f\Gamma$ be equal to the total energy dissipated per second in the viscous liquid, can be presented in the following form [39,40] (summation over repeating indices):

$$2\pi f\Gamma = \eta_{\text{eff}}\xi v^2 + \int dV [T_{ij}A_{ij} + (\mathbf{h}' \cdot \mathbf{N})]. \quad (1)$$

Here

$$\begin{aligned} \mathbf{N} &= \frac{\partial \delta\mathbf{n}}{\partial t} + (\mathbf{u} \cdot \nabla)\delta\mathbf{n} - \frac{1}{2}(\nabla \times \mathbf{u}) \times \mathbf{n}, \\ A_{ij} &= \frac{\partial u_i}{\partial x_j} + \frac{\partial u_j}{\partial x_i}, \\ h'_i &= \varepsilon_{ijk}(T_{jk} - T_{kj}), \\ T_{ij} &= T_{ij}(n_i, A_{ij}) \\ &= \alpha_2 n_j N_i + \alpha_3 n_i N_j + O(A), \end{aligned} \quad (2)$$

where ε_{ijk} is the unit antisymmetric tensor, $O(A_{ij})$ is a certain tensor linear in the tensor A_{kl} , and x_j are components of a vector in a Cartesian reference frame with the axis $x_3 = z$ along the spiral's axis \mathbf{n}_0 and $-\mathbf{v}$. The first term in (1) is the

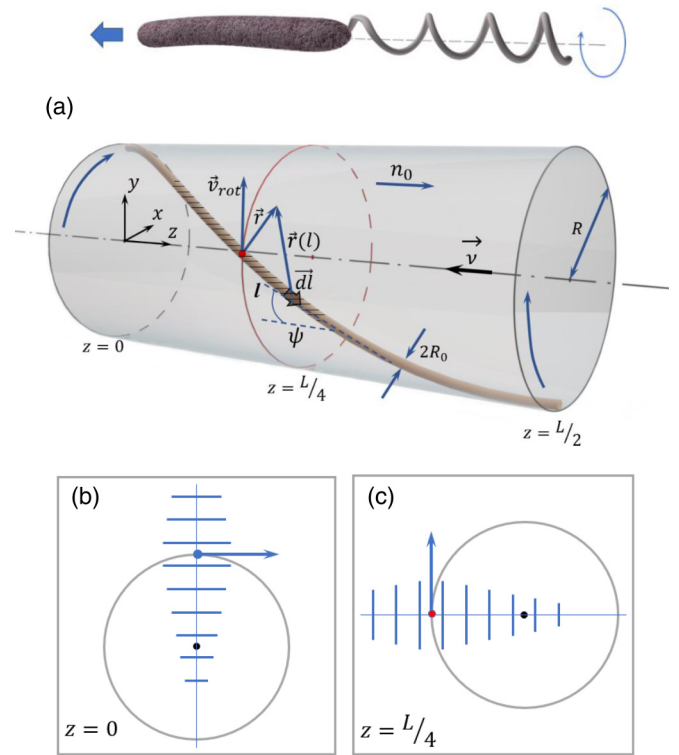


FIG. 5. Moving bacterium at an instant $t = 0$ [Eq. (8)] that rotates its helical flagellum of period L counterclockwise. Because of the planar anchoring on the surfaces of the bacterium's head and flagellum, the speed and flagellum's axis are along the unperturbed director \mathbf{n}_0 (along the z axis). (a) Half-period of the flagellum at instance $t = 0$. Its small element $d\mathbf{l}$ makes an angle ψ with the unperturbed director \mathbf{n}_0 and tends to align the director along itself. As a result, it induces some director distortion at a point in the plane $z = L/4$ a distance $r(l)$ from $d\mathbf{l}$ and a distance r from the flagellum. The shaded flagellum's segments of length $\sim R$ on both sides from the plane $z = L/4$ effectively contribute to the distortion in this plane. (b) The director distortion $\delta\mathbf{n}$ at $t = 0$ in the plane $z = 0$ is along the tangent to the base circle at the intersection with the flagellum. The distortion is shown on the line connecting the flagellum and its axis; its magnitude corresponds to the segments' lengths. (c) Same as in (b) but for the plane $z = L/4$.

dissipation due to the viscous drag force $\eta_{\text{eff}}\xi v$, where η_{eff} is the viscosity measured in the above experiment and ξ is the flagellum drag coefficient along the director (ξ has the dimension of length as it absorbs the effective size parameter that is not known for bacteria). The second term is the nematodynamic dissipation [39,40]. In general, the viscous nematodynamic dissipation has contributions $T_{ij}A_{ij}$ by shear flow and $h'_i N_i$ by director rotation. In our case of stationary motion, the balance equation can be simplified if only the terms linear in δn are retained. It is straightforward to verify that, in this linear approximation, the contraction $T_{ij}A_{ij}$ consists of terms proportional to $\delta_{i3}\partial u_j/\partial x_3$ or $\delta_{j3}\partial u_i/\partial x_3$ and, as in the stationary state, the velocity depends only on the distance from the z axis; these terms can be neglected. In the same approximation, the vector h'_i is obtained in the form

$$h'_i = \gamma_1 N_i, \quad (3)$$

where $\gamma_1 = \alpha_3 - \alpha_2$, with α_3 and α_2 two of the five independent Leslie coefficients [39]. Finally, we notice that $\nabla \times \mathbf{u} = \nabla \times \mathbf{v}_{\text{rot}}$ is parallel to \mathbf{n}_0 , so in the linear approximation $\nabla \times \mathbf{u} \times \mathbf{n} \approx 0$. In summary, the shear term TA and the $\nabla \times \mathbf{u}$ term in \mathbf{N} are neglected and the balance equation (1) takes the form

$$2\pi f\Gamma = \eta_{\text{eff}}\xi v^2 + \gamma_1 \int dV \left(\frac{\partial \delta \mathbf{n}}{\partial t} + (\mathbf{v} \cdot \nabla) \delta \mathbf{n} \right)^2. \quad (4)$$

Our idea is to estimate the director perturbation $\delta \mathbf{n}$ due to the anchoring on the flagellum surface, when possible make use of known experimental dependences of the material constants on the temperature T , and then find the velocity $v(T)$ from Eq. (4) of the energy balance.

B. Flagellum-induced director perturbation

One of the most striking feature observed in our and previous experiments [9] is that the bacterial flagellum, having a diameter of only a few tens of nanometers, produces director perturbations on the scale of micrometers (Fig. 4). Here we give a qualitative but quite general consideration of the perturbation $\delta \mathbf{n}$ of the homogeneous director \mathbf{n}_0 induced by a spiral flagellum.

The anchoring on a small element of the flagellum surface tends to align the director in its proximity along its easy axis. The easy axes at the flagellum of the *Proteus* are believed to be planar, tend to align the director along the flagellum, and thus are parallel to the unit vector \mathbf{l} of the local flagellum axis. In the first approximation, neglecting $\delta \mathbf{n}$, the anchoring energy dE_a of a small flagellum element dl is

$$dE_a = -\frac{W}{2} \int dS_l (\mathbf{n}_0 \cdot \mathbf{l})^2 = -\pi W R_0 dl \cos^2 \psi, \quad (5)$$

where W is the anchoring coefficient. The torque $d\Gamma_a$ exerted by this element on the director is the derivative

$$d\Gamma_a = -\frac{\partial dE_a}{\partial \psi} = \pi R_0 W dl \sin 2\psi [\mathbf{n}_0 \times \mathbf{l}]. \quad (6)$$

It is known that an external torque exerted on an object floating in a LC, e.g., a colloidal particle, makes it an elastic monopole that induces Coulomb-like director distortion [39,41,42]. The torque $d\Gamma_a$ thus plays the role of the vector of elastic charge of the element dl [41,42], the element becomes an infinitesimal elastic monopole, and the total director perturbation at a point \mathbf{r} due to the flagellum is a superposition of the fields induced by all these monopoles. In the one-constant approximation with the elastic constant K , the total flagellum-induced director distortion is given by the following integral along the flagellum [41,42]:

$$\begin{aligned} \delta \mathbf{n}(\mathbf{r}) &= \int \frac{[d\Gamma_a(l) \times \mathbf{n}_0]}{4\pi K |\mathbf{r} - \mathbf{r}(l)|} \\ &= \frac{R_0}{L_a} \sin 2\psi \int dl \frac{\mathbf{l}_\perp(l)}{4|\mathbf{r} - \mathbf{r}(l)|}. \end{aligned} \quad (7)$$

Here we introduced two important quantities, the anchoring extrapolation length $L_a = K/W$ and the vector $\mathbf{l}_\perp(l) = \mathbf{l}(l) - \mathbf{n}_0 \cdot \mathbf{l}(l)$, which is the component of the local flagellum axis $\mathbf{l}(l)$ normal to the director \mathbf{n}_0 . From the formula (7) we can derive the following properties of the perturbation $\delta \mathbf{n}(\mathbf{r})$ (Fig. 5).

First, it is everywhere normal to \mathbf{n}_0 . Further, the flagellum spiral lies on the cylindrical surface of the radius R . Consider some fixed cross section S_\perp of the spiral by the plane normal to its axis given by $z = L/4$. The point at which the spiral is piercing this plane lies on the circle of the cylinder base and moves along it with frequency f . Equation (7) implies that the perturbation vector $\delta \mathbf{n}$ lies in this plane and is parallel to the tangent to the base circle at the piercing point [Figs. 5(a) and 5(b)] so that the entire director rotates in this cross section along with the flagellum's point with frequency f . Thus, the overall director perturbation has the spiral form: It is concentrated in a tube centered at the flagellum axis and rotates along with it, its maximum magnitude being at the flagellum surface. Now consider a fixed Cartesian reference frame (x, y, z) with the z axis along the spiral's axis and suppose that, at an instant $t = 0$, the flagellum coordinates in the normal cross section $z = 0$ were $x = 0$ and $y = R$. Then the perturbation $\delta \mathbf{n}(t, x, y, z)$ has the form of the counterclockwise rotation

$$\begin{aligned} \delta \mathbf{n}(t, x, y, z) &= \delta n(r) \left[\mathbf{e}_x \cos \left(2\pi ft - \frac{2\pi z}{L} \right) \right. \\ &\quad \left. - \mathbf{e}_y \sin \left(2\pi ft - \frac{2\pi z}{L} \right) \right], \end{aligned} \quad (8)$$

where \mathbf{e}_x and \mathbf{e}_y are the orthogonal unit vectors in the normal-to- z plane (Fig. 5). Here $\delta n(r)$ is the magnitude and r is the distance from the flagellum to a point (x, y) in the plane $z = L/4$. Note that the z projection of the velocity \mathbf{v} is $-v$.

In the balance equation (4) $(d\delta \mathbf{n}/dt)^2$ appears, averaged over the above cross section S_\perp which needs to be estimated. Let us first find δn in a plane $z = \text{const}$. Clearly, the integral over the normal plane is that over the distance r of the function $\delta n(r)$. The flagellum is not straight; hence only its restricted neighboring segments contribute to δn in the plane S_\perp . As R is the only natural length associated with the flagellum turn, we set these segments, one on each side of the plane S_\perp , to be of length R . In any plane $z = \text{const}$ we have

$$\begin{aligned} \delta n(r) &\sim \frac{R_0 \sin 2\psi}{4L_a} \times 2 \int_0^R \frac{dl}{\sqrt{r^2 + l^2}} \\ &= \frac{R_0 \sin 2\psi}{2L_a} \ln \frac{R + \sqrt{R^2 + r^2}}{r}. \end{aligned} \quad (9)$$

The maximum $\delta n \propto \ln(2R/R_0)$ is at the flagellum surface and far from it, for large r , δn dies out logarithmically. Now we need to estimate the integral

$$\begin{aligned} \int dS_\perp \delta n^2 &\approx \left[\left(\frac{R_0}{L_a} \right) \sin 2\psi \right]^2 R^2 \\ &\quad \times \int_{R_0/R}^1 \left(\frac{\pi}{2} \right) r dr \left(\ln \frac{1 + \sqrt{1 + r^2}}{r} \right)^2. \end{aligned} \quad (10)$$

In the range $0.01 < R_0/R < 0.3$, the integral in the second line changes from 1.47 to 1.05 and we just set it equal to one, i.e.,

$$\int dS_\perp \delta n^2 \approx \left[R \left(\frac{R_0}{L_a} \right) \sin 2\psi \right]^2. \quad (11)$$

Combining (8) and (11), applying $d/dt = \partial/\partial t - v\partial/dz$ to $\delta \mathbf{n}$, and integrating along the flagellum length mL , it is

straightforward to get the second term in the balance equation (4):

$$m \int_0^L dz \int dS_{\perp} \left(\frac{d\delta n}{dt} \right)^2 \approx (4\pi)^2 m \left[R \left(\frac{R_0}{L_a} \right) \sin 2\psi \right]^2 \left(f^2 L + 2fv + \frac{v^2}{4L} \right). \quad (12)$$

With the result (12), the balance equation (4) can be reduced to the final form

$$Av^2 + Bv + C = 0. \quad (13)$$

Here

$$\begin{aligned} A &= \eta_{\text{eff}} \xi + \gamma_1 \sigma / L, & B &= \gamma_1 \sigma f, \\ C &= \gamma_1 \sigma f^2 L - 2\pi f \Gamma, \end{aligned} \quad (14)$$

where σ is the combination of the geometric parameters

$$\sigma = m \left[4\pi R \left(\frac{R_0}{L_a} \right) \sin 2\psi \right]^2. \quad (15)$$

C. Temperature dependence of the material parameters and fitting the experiment

The parameters entering the coefficients A , B , and C are certain functions of temperature and to solve Eq. (15) with respect to $v(T)$ we need their dependences explicitly. In what follows we indicate the parameters and data from the range $T \lesssim 15^\circ\text{C}$ by the index ‘‘con’’ as in this temperature range the regime is referred to as conventional. We will need our experimental dependences $v_{12,\text{con}}(T)$ and $v_{9,\text{con}}(T)$ for 12- and 9- μm bacteria, $f(T)$ and $\eta_{\text{eff}}(T)$,

$$\begin{aligned} v_{12,\text{con}}(T) &= 10^{-6} [0.65(T - 5) + 1.8] \text{ m/s}, \\ v_{9,\text{con}}(T) &= 10^{-6} [0.5(T - 5) + 1.2] \text{ m/s}, \\ f(T) &= [0.55(T - 5) + 1] \text{ s}^{-1}, \\ \eta_{\text{eff}}(T) &= 6 \exp[-0.18(T - 5)] \text{ Pa s}, \end{aligned} \quad (16)$$

where T is in the centigrade scale. We will also need the splay elastic constant $K_{11}(T)$ and the so-called twist (similar to splay) viscosity $\eta_{22}(T)$, which was measured in Ref. [19] for the LCLC used in our experiment. However, the data presented in [19] were obtained for the range from 21°C to 31°C , so we had no choice but to extrapolate these data to the temperatures of our experiment, i.e., down to 5°C . The thus obtained T dependences are

$$\begin{aligned} K_{11}(T) &\sim K_{33}(T) \sim 6 \times 10^{-10} \exp[-0.2(T - 5)] \text{ N}, \\ \eta_{22}(T) &= 3 \times 10^4 \exp[-0.4(T - 5)] \text{ Pa s}, \\ \eta_{33}(T) &\sim 10^{-3} \eta_{22} \ll \eta_{22}. \end{aligned} \quad (17)$$

Further, the data indicate that the torque Γ remains nearly constant in the conventional regime where the nematodynamic term is small and the torque can be estimated as $\Gamma_{\text{con}}(T) = \eta_{\text{eff}} \xi v_{\text{con}}^2(T) / f(T)$. This quantity, for both 12- and 9- μm bacteria, remains nearly constant up to 10°C when the LC effects can no longer be neglected. We assume that the torque Γ

remains constant in our experimental situation, which seems to be natural in the absence of additional information.

The viscous coefficient γ_1 is not reliably known for a LCLC. It Refs. [19,20] it was suggested that, since the term $\gamma_1(\mathbf{v}\nabla)\mathbf{n}$ [Eq. (4)] is related to director rotation, the constant γ_1 can be associated with the twist viscosity η_{22} , i.e., $\gamma_1 \sim \eta_{22}$.

The next important question is the ratio $L_a = K/W$. The deformation induced by the flagellum surface in its proximity consists of splay and bend. In the interval of T where the elastic constants K_{11} and K_{33} in [19] were measured, it was found that $K_{11} \sim K_{33}$, so we can take K_{11} for the average constant K . However, the behavior of the anchoring W with temperature has not been investigated in a LCLC. As the temperature dependence of K_{11} in our LCLC is exponential [see (17)], we assume an exponential dependence $L_a(T)$ and adjust the exponent to fit the experiment. Note that the product $\gamma_1 \sigma$ present in the coefficients A , B , and C contains the combination $\eta_{22} W^2 / K_{11}^2$, which is practically T independent if W varies slowly [see (17)].

The above consideration clearly shows that the available experimental data are highly insufficient for unambiguously choosing a few parameters that would have provided a good fit to the experimental curve $v(T)$. Therefore, we embark on the following approach. First, we choose the standard values for the flagellum’s parameters, such as its period L , spiral’s radius R , and flagellum’s radius R_0 , anchoring coefficient W , constant torque Γ , and drag coefficient $\xi = 2\pi \Gamma f(5) \eta_{\text{eff}}^{-1}(5) v_{\text{con}}^{-2}(5)$ [obtained for $T = 5^\circ\text{C}$ from (4)], and the number of periods m and then adjust the exponent of the dependence $L_a(T)$. We will see that this allows for a correct explanation of the central effect in the dependence $v(T)$, but not its periphery. Then we use this to understand what is missing in the T dependence of L_a assumed at the first step and make a further assumption. The result thus obtained shows that now the main mechanisms behind the velocity dependence on the viscosity and anchoring are correctly identified so that this can guide further development, e.g., in elucidating the very particular role of anchoring in active LCLC colloids.

Solving Eq. (13) with respect to the velocity, we obtain

$$v = \frac{-B + \sqrt{B^2 - 4AC}}{2A}. \quad (18)$$

In all the fits we keep $\psi = \pi/4$ and $m = 2$. First we describe bacteria of 12 μm size. For the first try fit, our choice consists of quite standard material constants [9] (see Fig. 3 and the Supplemental Material [43]): $R = 0.43 \mu\text{m}$, $R_0 = 0.13R$, $\Gamma = 6 \times 10^{-16} \text{ J}$, the correspondent $\xi = 1.94 \times 10^{-4} \text{ m}$, and $L_a = K_{11}/W = 20 \exp[-0.29(T - 5)] \mu\text{m}$. This fit is presented by the dashed curve $v_{0,12}$ in Fig. 6(a). It correctly describes the conventional regime and its crossover point to the aberrant one, but after passing the maximum value the velocity drops too fast. The reason is that the anchoring becomes too large as T exceeds $\sim 20^\circ\text{C}$. Indeed, if the anchoring in the second term in the coefficient C is divided by 10, then the theoretical curves $v_{\text{try},12}(T)$ and $v_{\text{try},9}(T)$ for this try fit, for both 12- and 9- μm bacteria, approach the experimental data [Fig. 6(a)]. For the 9- μm bacteria the only changes are $R' = 0.4 \mu\text{m}$, $R'_0 = 0.1R'$, and $\Gamma' = 9 \times 10^{-17} \text{ J}$.

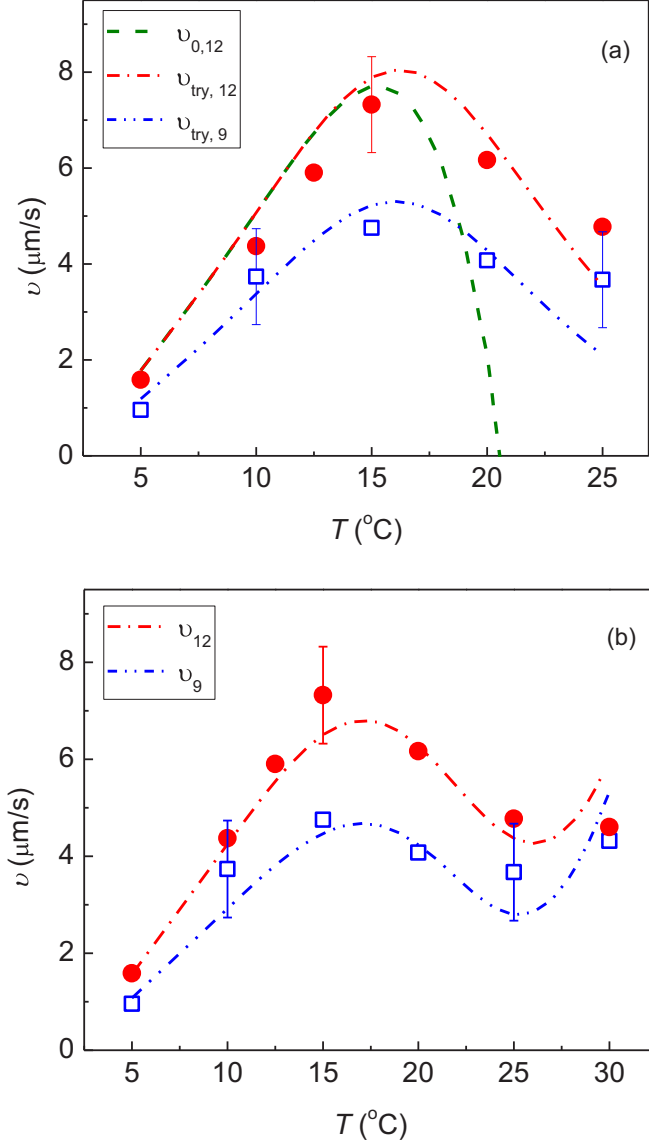


FIG. 6. Experimental temperature velocity dependences for 12- μm (circles) and 9- μm (squares) bacteria and theoretical fits (subscripts stand for bacterium size): (a) zero fit $v_{0,12}$ (dashed line) and try fit $v_{\text{try},12}$ (dash-dotted line) and $v_{\text{try},9}$ (dash-double-dotted line) and (b) fit (19) v_{12} (dash-dotted line) and v_9 (dash-double-dotted line).

Figure 7 presents the magnitude of the flagellum-induced director distortions $\delta n_{\text{max}} \sim (R_0 \sin 2\psi / 2L_a) \ln(R/R_0)$ [Eq. (9)] for 12- and 9- μm bacteria in the interval of temperatures from 5°C to 20°C for the above try fit. It shows that both δn_{max} sharply increase with T . The experimental fact that these distortions become better visible at $T \sim 15^\circ\text{C}$ implies that the value $\delta n_{\text{max}} \sim 0.06$ attained at this temperature for 12- μm bacteria is already detectable, while for 9- μm bacteria, $\delta n_{\text{max}} \sim 0.04$ is lower and its visibility is poorer.

Having realized that the experimental data point to the process in which, as temperature goes up, the anchoring is increasing progressively slower than was assumed above, we model the dependence of L_a by the following sets of param-

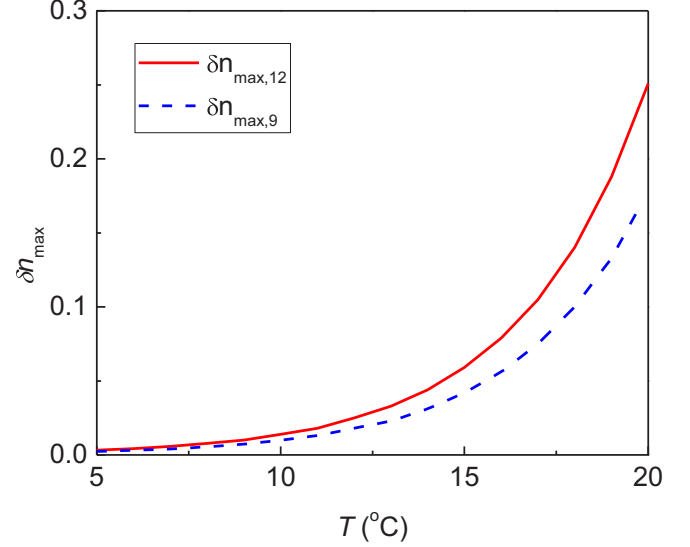


FIG. 7. Magnitude of the flagellum-induced director distortion δn_{max} for the 12- μm (solid line) and 9- μm (dashed line) bacteria found from the try fit.

eters (indices 12 and 9 stand for the bacterium size):

$$\begin{aligned}
 (\gamma_1\sigma)_{12} &= 3.28 \times 10^{-11} \frac{\exp[0.125(t-5)]}{1 + 0.06 \exp[0.2(t-5)]} \text{ J s}^2/\text{m}, \\
 (\gamma_1\sigma)_9 &= 2.41 \times 10^{-11} \frac{\exp[0.125(t-5)]}{1 + 0.06 \exp[0.204(t-5)]} \text{ J s}^2/\text{m}, \\
 \Gamma_{12} &= 6 \times 10^{-16} \text{ N}, \quad L_{12} = 2.9 \mu\text{m}, \\
 \Gamma_9 &= 4 \times 10^{-16} \text{ N}, \quad L_9 = 3.15 \mu\text{m}.
 \end{aligned} \tag{19}$$

The products $\gamma_1\sigma$ do not specify their constituents as this does not make much sense: Both $\gamma_1\sigma$ are on the order of that for the first try fit where all quantities were specified. The two T dependences are designed as to make the initially increasing function of T eventually decreasing. As these functions are proportional to W^2 , they model a similar process in the anchoring strength. Note that both T dependences have small positive exponents, which is in line with the fact mentioned above that without the T dependence of W , $\gamma_1\sigma \propto \eta_{22}/K_{11}^2$ would be practically constant. The exponents in the denominators that eventually result in the decrease of $\gamma_1\sigma$ are only slightly higher than those in the nominator which shows that the process might be tuned quite fine.

The fit for the sets (19) is presented in Fig. 6(b). In particular, it demonstrates that the tendency for an eventual linear velocity increase for higher T can be, at least in principle, accounted for in our approach.

IV. CONCLUSION

The theoretical fits to the experimental dependence $v(T)$ in Fig. 6 confirm that the nonmonotonic dependence of the bacterium speed on temperature and on viscosity is connected to the excitation of the elastic degrees of freedom of a nematic LC by the anchoring on the flagellum surface. We emphasize,

however, that the phenomenon reported in this paper, namely, that bacteria slow down in a nematic LC while the viscosity drops by orders of magnitude, is the effect peculiar for a lyotropic system where an extremely fast viscosity drop can be in a certain sense compensated by a compatible change of another parameter. In our case, this parameter is the splay elastic constant that drops exponentially with temperature, thus resulting in a dramatic increase of the flagellum's ability to induce director deformations. For this reason, temperature-induced effects such as variations of the viscosity anisotropy, propulsion torque, and flagellum geometry [44] should be ruled out as possible causes of the effect as these variations are incompatible with that of viscosity. The situation would be different in a thermotropic LC where L_a is proportional to the scalar order parameter S . An effect similar to that reported here would in principle also be possible there; however, as temperature variations of the viscosity [45,46], scalar order parameter, and the above parameters are compatible, all of them could contribute to the effect. Unfortunately, we will hardly ever see such an effect as bacteria cannot stay alive in nonaqueous thermotropic LCs.

To conclude, our results stress the important role the temperature dependence of the anchoring strength on the flagellum surface plays in bacteria self-propulsion. Anchoring is known to be a much harder problem in LCLCs as compared to that in thermotropic LCs. The fit (19) shows a plausible temperature dependence of the combination $\gamma_1\sigma \propto R_0^2W^2\eta_{22}/K_{11}^2$. This can be employed to extract the temperature dependence of the coefficient R_0W representing the effective flagellum anchoring strength and help to advance our understanding of bacteria propulsion.

ACKNOWLEDGMENTS

This research was supported by the National Academy of Sciences of Ukraine through Projects No. BC205, No. B197, and No. 6Φ-2018 and NRFU Project No. 2020.01/0144. The authors thank Zabolotny Institute of Microbiology and Virology of the NASU for providing the bacteria strains and equipment. We thank the anonymous referee for referring us to the physiological effect presented in Ref. [23].

-
- [1] C. J. Woolverton, E. Gustely, L. Li, and O. D. Lavrentovich, *Liq. Cryst.* **32**, 417 (2005).
- [2] A. Kumar, T. Galstian, S. K. Pattanayek, and S. Rainville, *Mol. Cryst. Liq. Cryst.* **574**, 33 (2013).
- [3] O. D. Lavrentovich, *Curr. Opin. Colloid Interface Sci.* **21**, 97 (2016).
- [4] M. M. Genkin, A. Sokolov, O. D. Lavrentovich, and I. S. Aranson, *Phys. Rev. X* **7**, 011029 (2017).
- [5] I. S. Aranson, *Phys. Usp.* **62**, 892 (2019).
- [6] C. Peng, T. Turiv, Y. Guo, Q. H. Wei, and O. D. Lavrentovich, *Science* **354**, 882 (2016).
- [7] T. Turiv, R. Koizumi, K. Thijssen, M. M. Genkin, H. Yu, C. Peng, Q.-H. Wei, J. M. Yeomans, I. S. Aranson, and A. Doostmohammadi, *Nat. Phys.* **16**, 481 (2020).
- [8] A. Sokolov, S. Zhou, O. D. Lavrentovich, and I. S. Aranson, *Phys. Rev. E* **91**, 013009 (2015).
- [9] Z. Shuang, A. Sokolov, O. D. Lavrentovich, and I. S. Aranson, *Proc. Natl. Acad. Sci. USA* **111**, 1265 (2014).
- [10] P. C. Mushenheim, R. R. Trivedi, H. H. Tuson, D. B. Weibel, and N. L. Abbott, *Soft Matter* **10**, 88 (2014).
- [11] J. Elgeti, R. G. Winkler, and G. Gompper, *Rep. Prog. Phys.* **78**, 056601 (2015).
- [12] E. Lauga and T. R. Powers, *Rep. Prog. Phys.* **72**, 096601 (2009).
- [13] M. S. Krieger, S. E. Spagnolie, and T. Powers, *Soft Matter* **11**, 9115 (2015).
- [14] J. S. Lintuvuori, A. Würger, and K. Stratford, *Phys. Rev. Lett.* **119**, 068001 (2017).
- [15] Ž. Kos and M. Ravnik, *Fluids* **3**, 15 (2018).
- [16] J. Dunstan, K. J. Lee, Y. Hwang, S. F. Park, and R. E. Goldstein, *Phys. Rev. Fluids* **3**, 123102 (2018).
- [17] M. S. Krieger, S. E. Spagnolie, and T. R. Powers, *J. Non-Newtonian Fluid Mech.* **273**, 104185 (2019).
- [18] A. Daddi-Moussa-Ider and A. M. Menzel, *Phys. Rev. Fluids* **3**, 094102 (2018).
- [19] S. Zhou, K. Neupane, Y. A. Nastishin, A. R. Baldwin, S. V. Shiyankovskii, O. D. Lavrentovich, and S. Sprunt, *Soft Matter* **10**, 6571 (2014).
- [20] S. Zhou, A. J. Cervenka, and O. D. Lavrentovich, *Phys. Rev. E* **90**, 042505 (2014).
- [21] J. Lydon, *Curr. Opin. Colloid Interface Sci.* **8**, 480 (2004).
- [22] W. R. Schneider, Jr. and R. N. Doetsch, *Appl. Environ. Microbiol.* **34**, 695 (1977).
- [23] M. Demir and H. Salman, *Biological J.* **103**, 1683 (2012).
- [24] H. Chi, M. Potomkin, L. Zhang, L. Berlyand, and I. S. Aranson, *Commun. Phys.* **3**, 162 (2020).
- [25] H. H. Tuson, M. F. Copeland, S. Carey, R. Sacotte, and D. B. Weibel, *J. Bacteriol.* **195**, 368 (2013).
- [26] I. Duchesne, S. Rainville, and T. Galstian, *Biophys. J.* **109**, 2137 (2015).
- [27] D. Nicolau, J. Armitage, and P. Maini, *Comput. Biol. Chem.* **33**, 269 (2009).
- [28] R. Stocker, *Proc. Natl. Acad. Sci. USA* **108**, 2635 (2011).
- [29] D. Kearns, *Nat. Rev. Microbiol.* **8**, 634 (2010).
- [30] J. Pande, L. Merchant, T. Krüger, J. Harting, and A.-S. Smith, *New J. Phys.* **19**, 053024 (2017).
- [31] Y. A. Nastishin, H. Liu, T. Schneider, V. Nazarenko, R. Vasyuta, S. V. Shiyankovskii, and O. D. Lavrentovich, *Phys. Rev. E* **72**, 041711 (2005).
- [32] V. G. Nazarenko, A. K. St. Clair, R. Klouda, R. D. Polak, Y. Nastishin, and O. D. Lavrentovich, *SID Int. Symp. Dig. Tech.* **29**, 135 (1998).
- [33] A. Kharina, O. Podolich, I. Faidiuk, S. Zaika, A. Haidak, O. Kukharenko, I. Zaets, F. Tovkach, O. Reva, M. Kremenskoy, and N. Kozzyrovska, *Basic Microbiol.* **55**, 509 (2015).
- [34] J. Manos, E. Artimovich, and R. Belas, *Microbiology* **150**, 1291 (2004).
- [35] H. P. Zhang, A. Be'er, E. L. Florin, and H. L. Swinney, *Proc. Natl. Acad. Sci. USA* **107**, 13626 (2010).

- [36] A. M. Menzel, A. Saha, C. Hoell, and H. Lowen, *J. Chem. Phys.* **144**, 024115 (2016).
- [37] J. Lighthill, *SIAM Rev.* **18**, 161 (1976).
- [38] M. Doi and S. F. Edwards, *The Theory of Polymer Dynamics* (Clarendon Press, Oxford, 1986).
- [39] P. G. de Gennes and J. Prost, *The Physics of Liquid Crystals* (Oxford Science, Oxford, 1993).
- [40] H. Stark, *Phys. Rep.* **351**, 387 (2001).
- [41] V. M. Pergamenschik and V. O. Uzunova, *Phys. Rev. E* **76**, 011707 (2007).
- [42] V. M. Pergamenschik and V. O. Uzunova, *Eur. Phys. J. E* **23**, 161 (2007).
- [43] See Supplemental Material at <http://link.aps.org/supplemental/10.1103/PhysRevE.104.054603> for details.
- [44] W. R. Schneider and R. N. Doetsch, *J. Bacteriol.* **117**, 696 (1974).
- [45] M. Cui and J. R. Kelly, *Mol. Cryst. Liq. Cryst.* **331**, 49 (1999).
- [46] H. Wang, T. X. Wu, S. Gauza, J. R. Wu, and S.-T. Wu, *Liq. Cryst.* **33**, 91 (2006).